Title: Peri-tumoural lymphocyte neighbourhoods predict longer survival in pancreatic ductal adenocarcinoma

Authors: Riley J. Arseneau[1,2], Jorge P. Mejia[2,3], Sarah Nersesian[2,3,&], Stacey N. Lee[3], Carley Bekkers[4], Thomas Samson[5], Daniel Gaston[1,2,4], Boris L. Gala-Lopez[1,2,3,6], Ravi Ramjeesingh[1,2,7], Thomas Arnason[1,4], Jeanette E. Boudreau[1,2,3]

Affiliations:

[1]Department of Pathology, Dalhousie University, Halifax, NS, Canada

[2]Beatrice Hunter Cancer Research Institute, Halifax, NS, Canada

[3]Department of Microbiology & Immunology, Dalhousie University, Halifax NS, Canada

[4]Department of Pathology and Laboratory Medicine, Nova Scotia Health Authority, Halifax, NS, Canada

[5]Faculty of Medicine, Dalhousie University, Halifax, NS, Canada

[6]Department of Surgery, Dalhousie University, Halifax, NS, Canada

[7]Division of Medical Oncology, Department of Medicine, Nova Scotia Health, Dalhousie University, Halifax, NS, Canada

[&]Current affiliation: Ottawa Hospital Research Institute, Ottawa, ON, Canada

* Address for correspondence:

Dr. Jeanette E. Boudreau

Jeanette.boudreau@dal.ca

5850 College Street, Room 15-F2, Halifax, NS, Canada, B3H 4R2

Running title: T cells predict longer survival in PDAC

Keywords: T cells, PDAC, Spatial Biology, pancreatic cancer, lymphocytes

Conflicts of interest: The authors declare they have no conflicts of interest

Word count: 5240

Number of Figures: 5

Number of tables: 1

Abstract

Background: Pancreatic ductal adenocarcinoma (PDAC) remains one of the deadliest cancers, and has limited options for treatment. Low immune infiltration, desmoplastic stroma, and poor tumour immunogenicity are all expected to contribute to PDAC's rapid progression and limited response to existing immunotherapies. PDAC tumours are mosaics of different sub-tumour microenvironments, including some that do contain immune cells. We hypothesized that increasing frequency of lymphocyte:tumour interactions would correlate with lengthened survival for patients with PDAC.

Methods: Using multiplex immunofluorescence, digital pathology, and computational analyses, we profiled the spatial distribution, co-localization, and neighbourhood architecture of immune cells in tumours from 73 patients with PDAC.

Results: Higher densities of CD3+CD8– (CD4+) T cells were associated with improved five-year overall survival, particularly when enriched at the tumour-stroma boundary (i.e. peritumoural). CD3+CD8- T cells, CD8+ T cells (CD3+CD8+), and B cells (CD20+) frequently co-infiltrated and co-localized, forming distinct immune neighbourhoods indicative of organized adaptive immunity. We defined three common immune neighbourhoods within PDAC (1) Macrophage-dominant; (2) T cell dominant; and (3) Disorganized. With greater tumour and peri-tumoural area represented by the T cell dominant neighbourhood, overall survival was increased. The other neighbourhoods were not significantly associated with outcomes.

Conclusion: Immune cells self-assemble in predictable patterns in PDAC. The presence of T cell dominant neighbourhoods, which we interpret as supporting ongoing immune activation, best predict lengthened survival. Spatially organized immune interactions may serve as prognostic indicators and inform future studies for immunotherapies in PDAC.

52 **Introduction**

53 Pancreatic ductal adenocarcinoma (PDAC) remains fatal in greater than 80% of patients, with few
54 options for effective treatment.[1] immunotherapies like immune checkpoint blockade or chimeric
55 antigen receptor (CAR)-T cells have transformed treatment of other cancers, such as melanoma and
56 leukemia,[2,3] but PDAC remains refractory to existing immunotherapeutic interventions.[4] PDAC is
57 often classified as an immunologically "cold" tumour, with a tumour microenvironment (TME)
58 marked by dense desmoplasia, poor immune cell infiltration, a low mutational burden/neoantigen
59 availability, and a high density of immunosuppressive cells such as M2 macrophages and regulatory
60 T cells (Tregs).[4,5] However, recent immunohistochemical assessments have revealed that PDAC is
61 heterogenous both within and between patients, a product of its "sub-TMEs".[6] Among these are
62 immune-enriched regions; this implies that immunity (and immunotherapy) remain possible in
63 PDAC.[6–10] In agreement, recent clinical investigations have demonstrated that neoantigen-targeting
64 personalized vaccines can drive effective cytotoxic T cell anti-tumour immunity in patients with
65 PDAC[11,12]. There is thus a need to better understand the immune microenvironment in PDAC: the
66 composition of tumour and immune cells and their spatial interactions may provide prognostic
67 insights that ultimately inform more precise care and future immunotherapies.

68 Immune-mediated tumour killing requires contact between tumour cells and cytotoxic
69 immune cells or their products (i.e. antibodies). Activation for anti-tumour immunity requires a co-
70 ordinated effort between immune cells that requires contact between antigen presenting cells,
71 helper T cells and effector lymphocytes. Increasingly, the spatial context of immune-tumour
72 interactions is being interrogated to better understand putative cell-cell communication, activation,
73 and priming—and predicting patient outcomes.[13–17] For example, tertiary lymphoid structures that
74 localize T cells, B cells, and antigen presenting cells enable anticancer immunity.[18] We recently
75 demonstrated that clusters of macrophages, T cells, and natural killer (NK) cells infiltrating the

76 tumour epithelial regions predicted the longest progression free survival in patients with high grade
77 serous carcinoma of the ovary.[16] The co-localization of immune cells with complementary functions
78 to collaboratively drive anticancer immunity best associated with patient survival, perhaps
79 underscoring a requirement for immune cell co-operation in tumour microenvironments.[16] Whether
80 a similar co-operation of immunity occurs in PDAC has not been investigated.

81 In this study, we used multiplex immunofluorescence (mIF) to assess the spatial
82 distribution, co-localization, and neighbourhood formation of macrophages, T cells, NK cells, and B
83 cells in 73 surgically-resected PDAC tumours. We designed a novel approach to segregate tumours
84 into epithelial, peri-tumoural and stromal regions, because unlike most solid tumours where there
85 is a clear delineation of tumour epithelium from its surrounding stroma, PDAC initiates in ducts and
86 metastasizes via small satellite tumour clusters.[19,20] We observed that enrichment of CD3+CD8– T
87 cells (likely CD4+ helper T cells) was associated with longer five-year overall survival (OS),
88 particularly when they are at the tumour-stroma (peritumoural) interface. The survival benefit was
89 further enhanced in patients with CD3+CD8- T cells in the stroma co-occurring with CD3+CD8+
90 (cytotoxic) T cells in the tumour epithelium, consistent with CD8+ T cell activation supported by
91 regional support from helper T cells. Unsupervised clustering revealed three patterns of immune cell
92 co-localization ("neighbourhoods"); one among them, containing CD3+CD8– T cells, CD3+CD8+ T
93 cells, and B cells, was associated with the best outcomes for patients. This neighbourhood may
94 represent regions of organized adaptive immunity and their presence in PDAC could therefore
95 represent a productive anti-cancer response. Hence, these T cell-enriched areas may inform patient
96 prognosis or precision medicine. While functional assessments will be required to determine the
97 specific anti-cancer activities and driving features of these neighbourhoods, their presence
98 underscores optimism for future, novel immunotherapies to support cytotoxic immunity in PDAC.
99

100 **Methods**

101 **Patient samples**

102 Samples were obtained from 76 patients with PDAC who underwent surgical resection from 2013 to
103 2024 at the Queen Elizabeth II Health Sciences Centre (Nova Scotia, CAN). This study was approved
104 by the Nova Scotia Health institutional research ethics board (#1023467 & #1026628). Patients who
105 received neoadjuvant therapy were excluded. Patient information is available in **Supplementary**
106 **Table 1.**

107 Patient samples were formalin-fixed, paraffin-embedded (FFPE) and assembled into tissue
108 microarrays (TMA). Each patient was represented by duplicate 3 mm cores selected from regions
109 containing >30% tumour cells, as identified by board-certified pathologist (TA).

110

111 **Multiplex immunofluorescence**

112 Opal mIF (Akoya Biotechnology, Marlborough, USA) was performed as previously described.[16]
113 Briefly, 4 µm sections were prepared from the TMAs, deparaffinized in Xylene (Sigma-Aldrich) (3 x 10
114 min) and rehydrated by incubating with decreasing concentrations of ethanol for 10 min each (100%,
115 100%, 95%, 70%). The slides were then fixed in 10% neutral buffered formalin (VWR) for 20 min.

116 The slides underwent serial cycles of antigen retrieval, primary staining, and tyramide signal
117 amplification to add each antibody and fluorophore one by one. For antigen retrieval, slides were
118 microwaved in Tris-EDTA buffer (pH9) at 1000W for 2 min, then 200W for 15 min. The slides were
119 cooled on ice for 10 min and rinsed in deionized water and Tris-buffered saline with Tween-20 (TBS-
120 T). Slides were thereafter blocked in 1x antibody diluent/block (Akoya Biosciences) for 10 min, the
121 excess block was removed, and the slides were stained with diluted primary antibody for 45 min.
122 After TBS-T rinsing, slides were incubated in secondary anti-mouse plus rabbit antibodies
123 conjugated to horseradish peroxidase (HRP) for 10 min. Signal amplification was completed via HRP-

124 driven tyramide activation and fluorophore deposition and tissue binding (Opal 6-Plex Manual
125 Detection Kit, and Opal 480 Reagent Pack (Akoya Biosciences)). Opal 780 staining (Opal 780 Reagent
126 Pack, Akoya Biosciences) required use of digoxygenin labeling prior to tyramide signal amplification
127 (10 min, TSA Plus DIG, Akoya Biosciences). The slides were rinsed in TBS-T and subsequently
128 incubated in the corresponding Opal fluorophore diluted in Opal amplification diluent for 10 min
129 (Opal 480, 520, 540, 570, 620, 650, and 690 fluorophores) or 1h (Opal 780). After the final staining
130 step, slides were counterstained with Spectral DAPI (ThermoFisher) for 10 min, rinsed, and mounted
131 in Mowiol-based mounting medium (Mowiol, glycerol, deionized H_2O, TrisHCl (pH 8.5); Sigma-
132 Aldrich)). Antibodies, Opal fluorophores with which they were used, and staining order are shown in
133 **Table 1**.

134 Antibody staining was validated using FFPE tonsil tissue and cell pellets of purified T and NK
135 cells. T and NK cells were isolated from primary peripheral blood mononuclear cells (Canadian
136 Blood Services, Dalhousie REB 2016-3842), centrifuged at 300 x *g* for 5 min, fixed in 10% neutral
137 buffered formalin, and processed for paraffin embedding. All staining patterns were confirmed by a
138 board-certified pathologist (TA). Representative images from one case and the segmentation
139 pipeline are shown in **Figure 1A**.

Table 1. Staining panel and order for mIF				
Phenotype	**Marker**	**Clone**	**Dilution**	**Fluorophore**
NK cells	CD57	NK1	1/50	650
M2 Macrophage	CD163	ERP19518	1/200	540
Macrophage/monocyte	CD68	SP251	1/100	690
Epithelial Cell	PanCk	AE1/AE3	1/100	520
Pan T cell	CD3	LN10	1/50	480
NK cells/monocyte	CD16a	SP175	1/50	620
Cytotoxic T cell	CD8	C8/144	1x	480
B cell	CD20	L26	1/25	780
DAPI (nuclear stain)	DAPI	N/A	15 μM	N/A

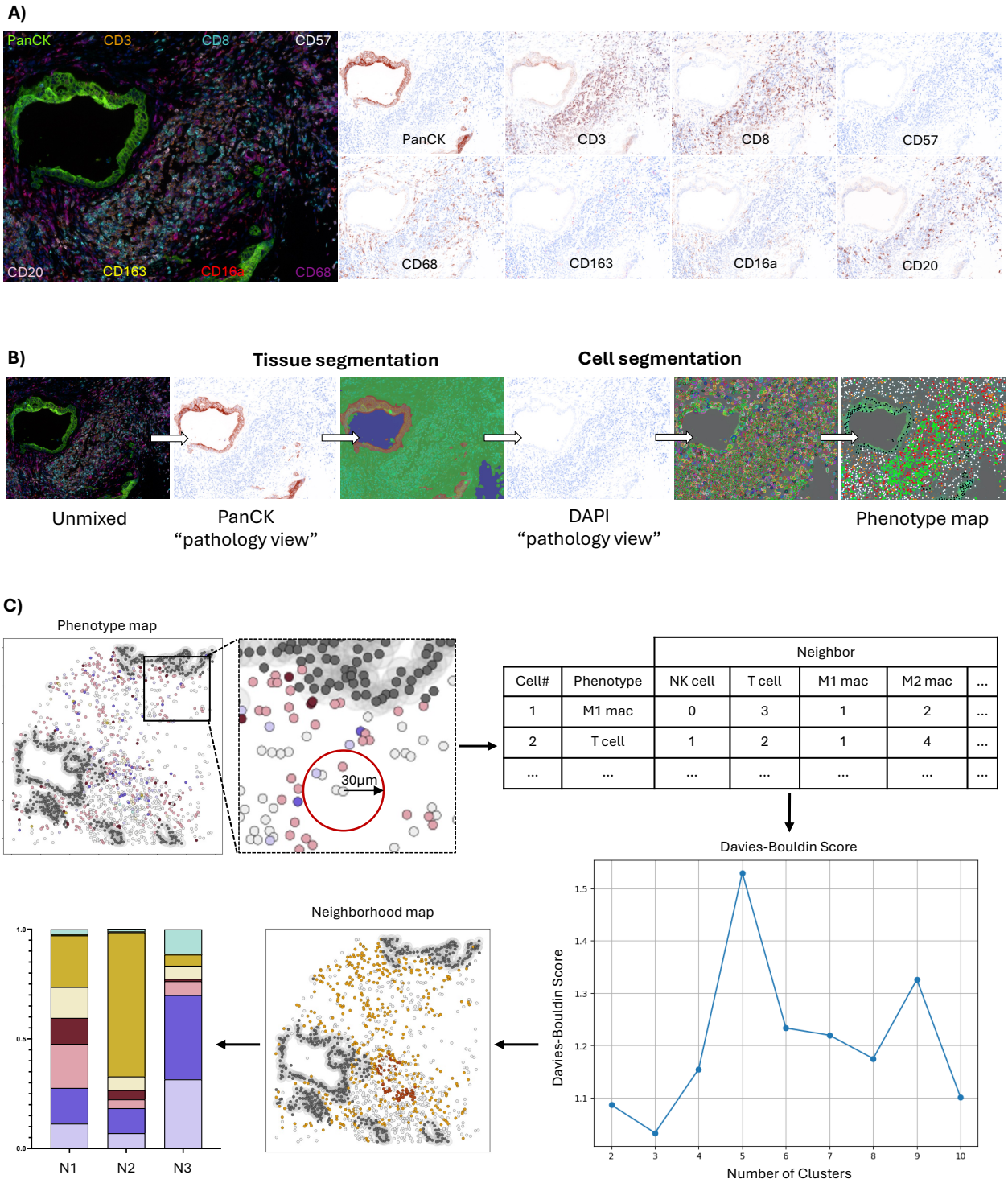

Figure 1. Quantitative image and neighbourhood analysis workflows. A) Fluorescent microscopy image using 9-colour mIF. Markers used include DAPI (blue), CD3 (orange), CD8 (cyan), CD57 (white), CD16a (red), CD68 (magenta), CD163 (yellow), CD20 (pink), and panCK (green). Representative pathology views for each marker are shown. **B)** Quantitative pathology workflow with tissue and cell segmentation based on PanCK and DAPI staining, respectively. **C)** x,y coordinates were used to reconstruct maps of tumours *in silico*. Cell groups were defined as at least five cells within a 30 µm

147 radius and k-means clustering identified cell neighbourhoods. Davies-Bouldin indexing was used to
148 define the ideal number of neighbourhoods, whose cellular compositions are reported as bar
149 graphs.
150
151 Imaging was completed using a Mantra Quantitative Pathology workstation equipped with
152 after-market Opal 480 and Opal 780 filter cubes. Images were acquired at 20x magnification, with
153 wavelength intervals spanning emission peaks between 420 nm and 780 nm to capture all Opal
154 fluorophores. Up to 15 images per core were captured, with multispectral analysis performed in
155 InForm Tissue Finder Software (Version 2.4.8). Spectral reference libraries, generated from
156 monoplex stains for each fluorophore, were used for spectral unmixing to distinguish fluorophore
157 signals and control for autofluorescence. Regions of benign panCK+ staining were omitted and
158 regions of tumour epithelium were confirmed by a board-certified pathologist (TA).
159 Using machine learning algorithms, tissue segmentation was performed on spectrally
160 unmixed images to distinguish epithelial and stromal regions (off-core regions were omitted and
161 could be distinguished from stroma by lack of DAPI staining and tissue autofluorescence). Nuclear
162 segmentation (DAPI) followed, and cell phenotypes were assigned by antibody staining. Phenotype
163 maps with x,y cell coordinates classified each cell with a unique cell ID **(Figure 1B)**. Cell types were
164 classified based on antibody expression profiles: panCK+ as epithelial cells (regardless of other
165 antibody binding), PanCK-CD68+ as macrophages (CD163+/– , CD16a+/–), PanCK–CD68–CD3+ as T
166 cells (CD8+/–, CD16a+/–, CD57+/–), PanCK–CD3–CD68–CD57+ as NK cells (CD16a+/–), PanCK–
167 CD3–CD68–CD57–CD16a+ as CD16a+ cells, and panCK–CD3–CD68–CD20+ as B cells. Cells
168 staining with DAPI only were categorized as "Other". Antibody binding patterns, cell surface staining,
169 cell segmentation, and phenotyping were validated by a board-certified pathologist (TA).
170 Quality control involved visual assessment of every image and excluding images with poor
171 tissue quality or non-specific staining. All quality control was performed blinded to clinical outcome

172 data. Of the 76 patients intended for study, images from 73 patients passed staining and quality
173 control and were included in the final analysis.
174
175 **Cell densities and spatial analyses**
176 *Cell densities*
177 Cell identities and x,y coordinates were exported from InForm. Cell densities were calculated in
178 RStudio (Boston, MA USA, version 2022.12.0) using the dplyr package.[21] For each patient, total
179 counts of each cell type between duplicate cores within the epithelial and stromal compartments
180 were summed and divided by the corresponding tissue area, resulting in region-normalized average
181 densities per patient (cells per mm^2). For cell-, neighbourhood, and region-level analyses, we
182 calculated the density (cells/mm^2) of each immune cell subset (or neighbourhood) per patient.
183 Density distribution curves were generated using the density () function in base R, and the division
184 into "high" and "low" densities was defined by the maxima, minima, or inflection point closest to the
185 median of each distribution.
186
187 *T cell infiltration score*
188 We generated a T cell infiltration score, following an approach like that used in Immunocore algorithm
189 used in colorectal cancer.[22,23] The T cell infiltration score ranged from 0 to 6 and was calculated by
190 summing binary high/low infiltration designations of CD3+CD8+ and CD3+CD8– T cells across the
191 epithelial and stroma compartments. Informed by compartment specific role of each subset,[24–27] we
192 assigned a greater weight to the subset most biologically relevant in each region. Patients received
193 two points for high CD3+CD8– T cell infiltration in the stroma and one point for high CD3+CD8+
194 infiltration in the stroma. Conversely, high CD3+CD8+ infiltration in the epithelium contributed two

195 points, while CD3+CD8– in the epithelium contributed one point. Patients were stratified into three
196 groups based on total score: low (0 points), intermediate (1-3 points), and high (4-6 points).
197
198 *Neighbourhood analysis*
199 Our spatial biology workflow was adapted from previously published methods[15,16] and conducted in
200 Python (Version 3.9.18). X,y coordinates of each cell were used to reconstruct phenotype maps of
201 tumours, and each cell was defined as an index. Cell IDs with their x,y coordinates and assigned
202 phenotypes were grouped by image and patient using Pandas[28] (for data organization and
203 manipulation) and NumPy[29] (for numerical operations). Using the BallTree module from scikit-
204 learn[30], for each index cell, cells within a 30 μm radius were identified based on their x,y, coordinates
205 (nearest neighbour search), defining local "groups" **(Figure 1C)**. To identify patterns of immune cell
206 co-localization, which we termed "neighbourhoods", three images from each patient were randomly
207 selected and combined to create a training set. Using this set, K-means clustering through
208 MiniBatchKMeans algorithm (scikit-learn) was applied to the immune cell populations only, testing
209 between 2 and 10 potential neighbourhoods. The optimal number of neighbourhoods to represent
210 intra-tumour diversity was defined using Davies-Bouldin indexing (scikit-learn).[31]
211 All remaining images were classified using the trained model to assign each cell to a
212 neighbourhood. To ensure neighborhood definitions reflected immune cell organization (not tumour
213 or other cells), epithelial (PanCK+) and "Other" cells were excluded from the clustering and instead
214 assigned to distinct "PanCK" and "Other" neighborhoods. This approach preserved their spatial
215 position in the radius-based analysis while preventing them from influencing immune
216 neighbourhood structure. Consistency of neighbourhood classification was validated by calculating
217 cosine similarity (scikit-learn), which scored >0.99 between the initial training set and the
218 subsequent classified images. Figures were generated with matplotlib[32] and seaborn[33].

219

220 *Tumour neighbourhood analysis*

221 To define tumour regions as intratumoural, peritumoural, and stromal, cell clustering was performed
222 in Python using the DBSCAN[34] and SciPy[35] packages. Epithelial (panCK+) cells were first identified in
223 each sample, and DBSCAN clustering was performed on these cells using a 30 μm radius and a
224 minimum cluster size of five cells. Cells that did not meet this clustering criteria were excluded from
225 defining intratumoural regions. SciPy's ConvexHull class was used to define the smallest bounding
226 shape (convex hull) for each tumour cluster, with visual confirmation by a pathologist (TA). Based on
227 these boundaries, three regions were defined: (1) Intratumoural: the area formed by each tumour
228 site; (2) Peritumoural: a 30 μm perimeter surrounding each tumour site; or (3) Stromal: the area
229 outside the intratumoural and peritumoural regions. Cell counts for each region were aggregated by
230 radius for each patient, and patients were subsequently classified into high and low groups based on
231 the proportion of each immune phenotype within the defined regions, as defined above.

232

233 **Statistical analysis**

234 To define which clinical variables were associated with survival and therefore should be used as
235 covariates for downstream multivariate analysis, we performed univariate Cox proportional hazard
236 regressions using five-year OS as the dependent variable in RStudio. Independent variables were
237 tumour stage, tumour grade, age at diagnosis, sex, and lymph node invasion **(Supplemental Table**
238 **S1)**. Among them, only increased regional lymph node metastasis was significantly associated with
239 shorter five-year OS ($p < 0.05$).

240 Univariate Kaplan-Meier and log-rank tests were conducted to assess differences in OS
241 between high and low groups of cell-, neighborhood-, and regional- analyses, and multivariate Cox
242 proportional hazards models were used to identify independent prognostic factors. Co-infiltration

243 between cellular phenotypes were assessed using Spearman's rank correlation in GraphPad Prism
244 (GraphPad Software, Boston, MA USA, version 10.2.3). Comparisons of immune cell infiltration
245 across clinically defined groups, including tumour stage (T1, T2, T3), tumour grade (1, 2, 3), age (<65,
246 ≥65), sex (male vs female), and regional lymph node metastasis (N0, N1, N2), were conducted using
247 two-tailed Mann-Whiteney U tests in GraphPad Prism, with corrections for false discovery to account
248 for multiple comparisons. Statistical significance was defined as an alpha of 0.05 for all analyses.

249 **Results**

250 *Patient characteristics*

251 Using Opal mIF, we evaluated tumours from a total of 73 patients with PDAC who underwent surgical
252 resection between 2013 and 2024 at the QEII Health Sciences Centre. Forty-five percent of the
253 cohort was female; 55% were male **(Supplemental Table 1)**. Most patients were >65 years old (59%,
254 n=43), and categorized as stage II (33%) or stage III (62%). Moderately differentiated tumours were
255 most common (63%, grade 2), followed by poorly differentiated (23%, grade 3), and well-
256 differentiated tumours (14%, grade 1). Regional lymph node involvement was most commonly
257 present: just 14% had no positive lymph nodes (N0), 60% of patients had 1-3 positive lymph nodes
258 (N1), and 21% having ≥4 nodes (N2). Patients with N0 disease had a lower risk of death compared to
259 N2 (HR: 0.16, 95% CI: 0.04-0.73, $p<0.05$). Since this was the only clinical variable associated with
260 OS, it was the only one included in downstream multivariate analyses.

261

262 *Immune architecture of PDAC microenvironment*

263 The immune microenvironment of PDAC is immunosuppressive and spatially heterogenous, yet
264 remains poorly characterized, with limited knowledge of how it reflects patient prognosis.[4,5] To
265 characterize the immune landscape of PDAC, we quantified immune cell densities (cells/mm^2) in
266 both the epithelial and stromal compartments using multiplex IHC and quantitative pathology
267 **(Figure 1)**. Tumours displayed marked immune infiltration with inter- and intra-patient heterogeneity
268 **(Figure 2A)**. Regardless of phenotype, immune cell densities were higher in the stroma than in the
269 epithelial compartment, likely reflecting limited accessibility to the tumour **(Figure 2A)**. Among
270 immune populations, the most abundant were CD16a+ M2-like macrophages (epithelium median:
271 11.3, min-max: 0-280.1; stroma median: 569.1, min-max: 45.2-4602.0) and CD3+CD8+ T cells
272 (epithelium median: 10.6, min-max: 0-216.1; stroma median: 234.4, min-max: 24.9-1446.0),

reflecting substantial infiltration in both compartments **(Figure 2A, Supplemental Table 2).** To reduce complexity and improve interpretability, populations with a median cohort total density of <1 cell/mm^2 were grouped into higher-level phenotypes based on shared marker expression **(Supplemental Table 2)**. Specifically, PanCK–CD68–CD3+CD8–CD57+ and PanCK–CD68–CD3+CD8–CD16a+ subsets were amalgamated into a CD3+CD8– T cell group; PanCK–CD68–CD3+CD8+CD57+ and PanCK–CD68–CD3+CD8+CD16a+ subsets were grouped as CD3+CD8+ T cells; and PanCK–CD68–CD3-CD8–CD57+CD16a– and PanCK–CD68–CD3-CD57+CD16a+ subsets were grouped as NK cells.

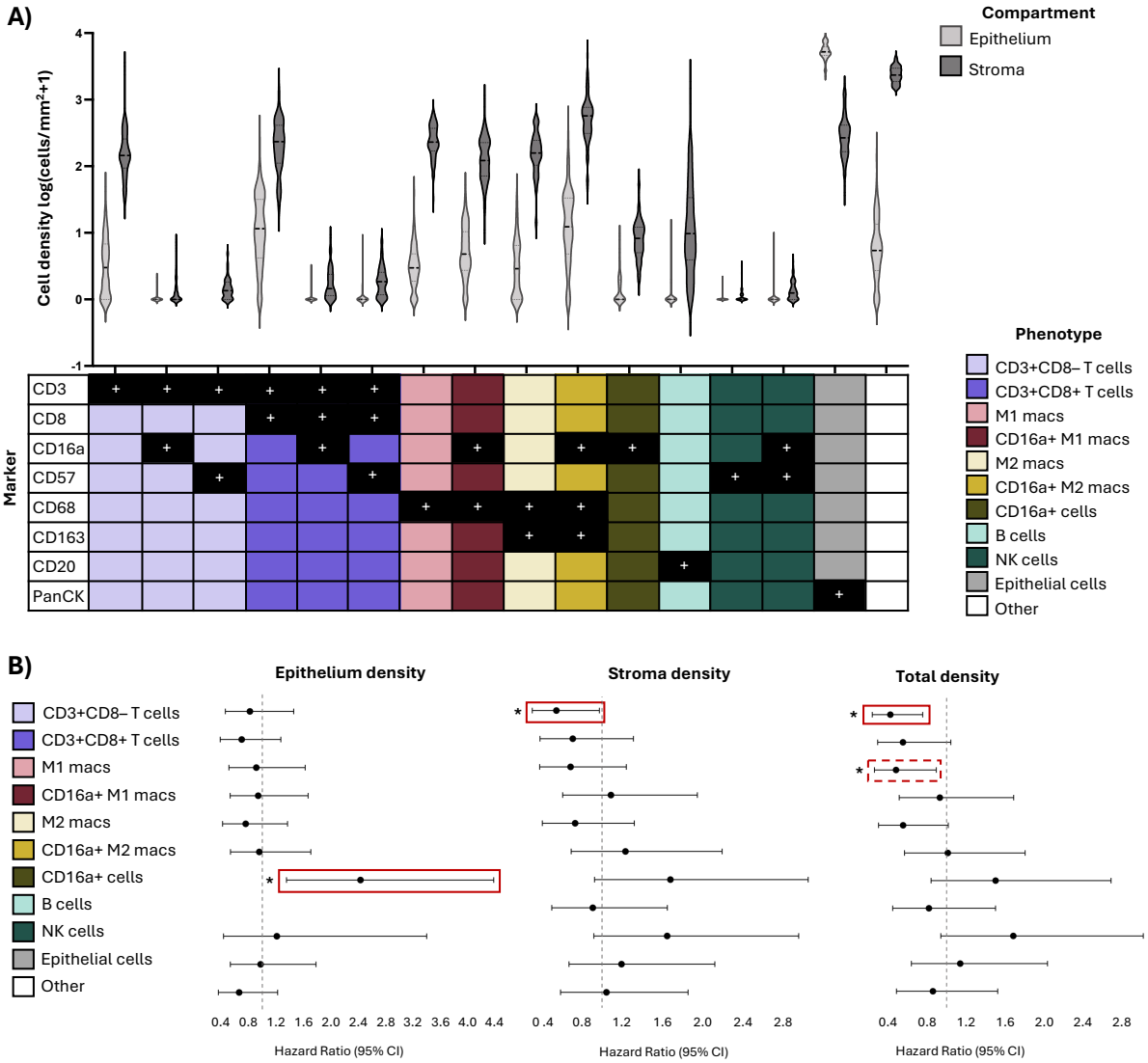

Figure 2. Immune cell frequencies and associations with survival. (A) Violin plots showing the densities of individual immune cell phenotypes within the stromal and epithelial compartments of PDAC cores. The table below indicates the marker expression profile for each phenotype, with black squares with "+" denoting marker positivity and colours representing aggregate cell phenotypes employed in downstream analysis. **(B)** Forest plots of hazard ratios from univariate Cox regressions comparing high vs low densities of each phenotype. Solid red boxes indicate phenotypes significant in both univariate and multivariate models; dotted red boxes denote phenotypes significant in univariate analysis only.

Increased T cell density is associated with greater overall survival.

Previous studies indicated that T cells, B cells, and macrophages, and their specific subsets inform good or bad prognosis in PDAC,[36–39] thus we sought to determine whether immune cell densities in PDAC tumour compartments correlated with OS. We used univariate and multivariate Cox regression analyses to compare 5-year OS in patients with immune cell densities categorized as high or low.

By univariate analysis, higher densities of epithelial CD16a+ cells were associated with an increased risk of death (HR: 2.4, 95% CI: 1.4–4.4, $p<0.05$), while higher densities of CD3+CD8– T cells in both the stroma and total tissue compartments were significantly associated with reduced risk of death (HR: 0.55, 95% CI: 0.31–0.97, $p<0.05$; HR: 0.42, 95% CI: 0.24–0.75, $p<0.05$, respectively) **(Figure 2B)**. These associations remained significant after adjusting for regional lymph node involvement by multivariate assessment (epithelial CD16a+: HR: 2.1, 95% CI: 1.1-3.9, $p<0.05$; stromal CD3+CD8-: HR: 0.47, 95% CI: 0.26-0.85, $p<0.05$); total CD3+CD8-: HR: 0.43, 95% CI: 0.24-0.80, $p<0.05$) **(Supplemental Table 3)**. Increased M1-like macrophage density was associated with decreased risk of death in univariate analysis (HR: 0.48, 95% CI: 0.26–0.89, $p<0.05$), but this association was lost in the multivariate model (HR: 0.55, 95% CI: 0.30-1.0. Thus, immune cell infiltration itself does not suggest improved prognosis: different subsets are variably prognostic and CD3+CD8– T cells may be a marker of improved OS in patients with PDAC.

Combined CD3+CD8– and CD3+CD8+ T cells infiltration is associated with improved OS

310 Immune cells function as a coordinated network. We next hypothesized that the association of
311 CD3+CD8- T cells with improved OS might reflect a role for these cells–which are likely helper T cells–
312 in supporting anti-tumour immune functions, including that of cytotoxic (CD3+CD8+ T cells). Indeed,
313 patients with high infiltration of both CD3+CD8- and CD3+CD8+ T cell subsets exhibit significantly
314 improved OS compared to those low for both (HR: 0.33, 95% CI: 0.12–0.88, $p<0.05$). While high
315 infiltration of either subset alone trended toward lengthened OS, neither reached statistical
316 significance (CD3+CD8– only: HR: 0.45, 95% CI: 0.17-1.2, $p=0.14$; CD3+CD8+ only: HR 0.65, 95% CI:
317 0.14-3.0, $p=0.88$) **(Figure 3A)**. Notably, high infiltration of CD3+CD8+ T cells alone was uncommon
318 (7% of patients) **(Figure 3B)**. These findings suggest that co-infiltration of helper and cytotoxic T cells
319 might enable local generation of antitumour immunity.

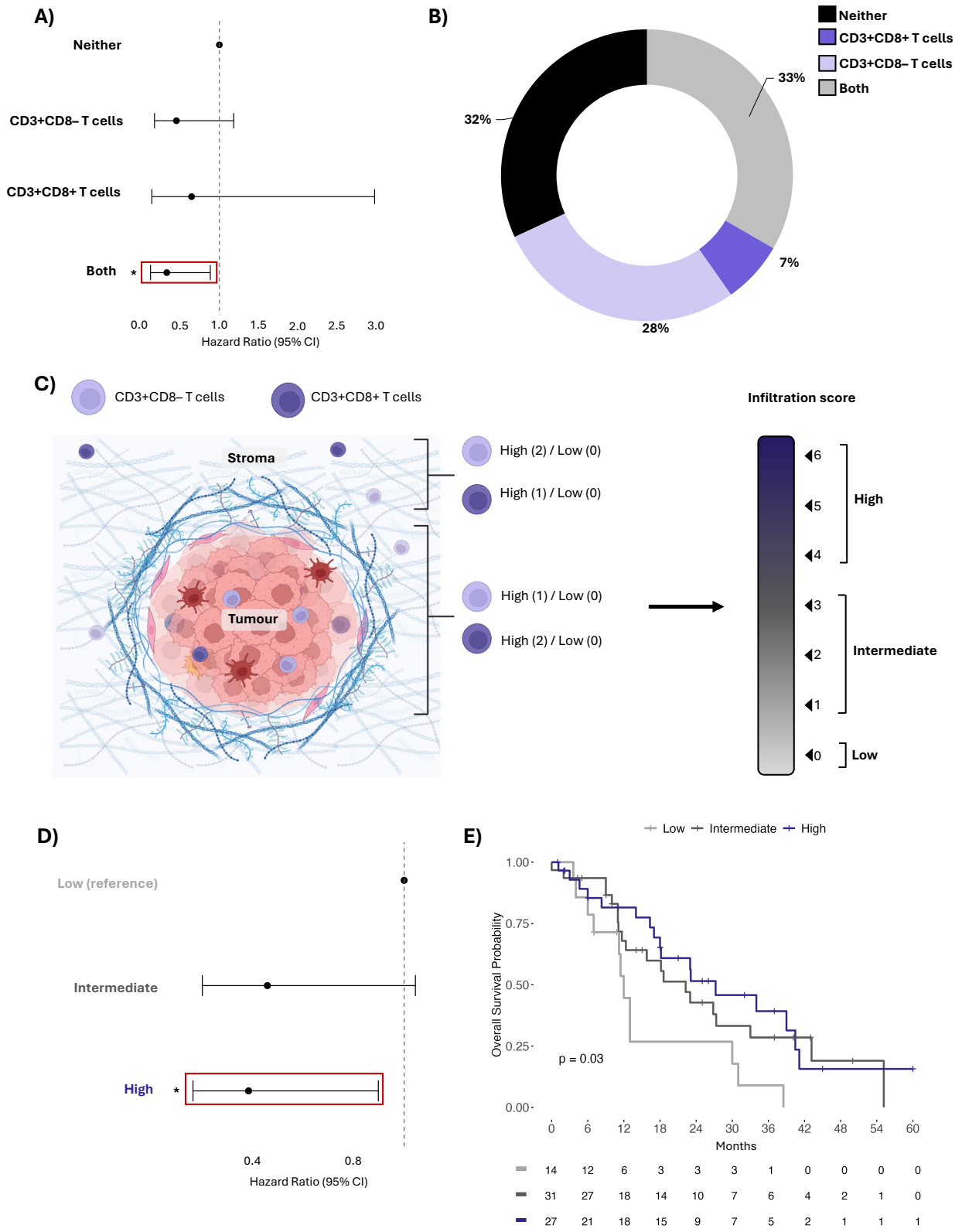

Figure 3. Combined CD3+CD8- and CD3+CD8+ T cell infiltration is associated with improved OS. (A) Forest plot showing hazard ratios and 95% confidence intervals from univariate Cox

regression comparing patients categorized as high for CD3+CD8+ only, CD3+CD8- only, both, or neither, based on total cell density. **(B)** Pie chart representing the percentage of patients in each T cell group. **(C)** Schematic of the T cell infiltration score. Created in BioRender. Arseneau, R. (2025) https://BioRender.com/teuxamp **(D)** Forest plot showing hazard ratios and 95% confidence intervals from univariate Cox regression comparing patients based on infiltration score (low, intermediate, and high). Kaplan-Meier survival plot comparing the five-year OS among patients stratified by infiltration score.

High T cell infiltration score is predictive of longer OS

CD8+ cytotoxic T cell killing is contact-dependent, but helper T cells can function from a distance. To evaluate whether compartment-specific localization influences prognosis, we generated a T cell score **(Figure 3C)**. High T cell infiltration scores were associated with reduced risk of death and improved survival compared to low in both univariate and multivariate Cox regression models (HR: 0.39, 95% CI: 0.16-0.90, $p<0.05$) and Kaplan-Meier survival analysis ($p<0.05$) **(Figure 3D&E, Supplemental Table S3)**. Patients with intermediate T cell infiltration scores exhibited a trend towards decreased risk of death and lengthened OS compared to those with low scores, though the difference did not reach statistical significance (HR: 0.46, 95% CI: 0.20-1.0, $p=0.066$) **(Figure 3D&E)**. These findings suggest that the localization of T cell subsets with respect to tumour cells impact patient prognosis.

Higher peritumoral CD3+CD8– T cell density corresponds to decreased risk of death

PDAC tumours grow as cells around pancreatic ducts, dispersed between dense stroma throughout the pancreas; this is different from other solid tumours where groups of cancerous cells aggregate.[19,20] Dichotomizing tumour versus stroma, as with other tumours, might therefore inadequately capture immune:tumour interactions in PDAC. To refine the assessment of spatial immune localization and its association with survival, we applied DBSCAN-based spatial clustering to segment tissue into intratumoural, peritumoural, and distal stromal regions and measure immune

cell localization within them **(Figure 4A).** This approach enabled a more granular evaluation of immune cell positioning at the tumour-stroma interface.

Within the intratumoural region, higher proportions of NK cells were associated with increased risk of death (HR: 2.6, 95% CI: 1.4-4.7, p<0.05) **(Figure 4B, Supplemental Table 3)**. Similarly, increased NK cell infiltration in the peritumoural space was also associated with worse survival (HR: 2.3, 95% CI: 1.2-4.2, p<0.05). In contrast, higher proportions of CD3+CD8-T cells in the peritumoural region were significantly associated with reduced risk of death (HR: 0.55, 95% CI: 0.30-0.99, p<0.05). Within the distal stroma, both CD3+CD8– and CD3+CD8+ T cells were associated with improved OS (HR: 0.53, 95% CI: 0.29-0.94, p<0.05; HR: 0.53, 95% CI: 0.29-0.95, p<0.05). Taken together, these findings suggest that T cell localization, particularly at the tumour-stroma interface, is predictive of prognosis in PDAC.

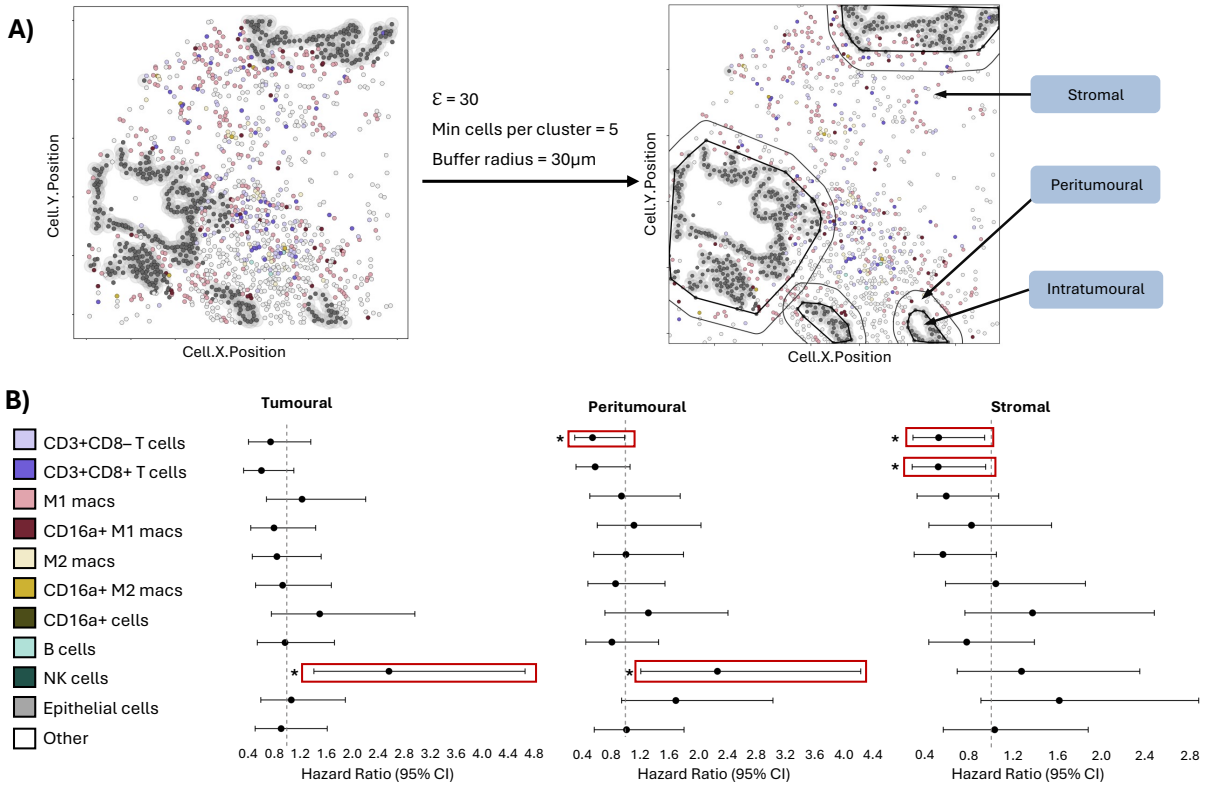

Figure 4. Immune cell proximity to the tumour predicts survival. (A) Schematic of DBSCAN-based clustering analysis. **(B)** Forest plots of hazard ratios from univariate Cox regressions comparing high

364 vs low proportions of each phenotype in each region. Solid red boxes indicate phenotypes significant
365 in both univariate and multivariate models; dotted red boxes denote phenotypes significant in
366 univariate analysis only.
367

368 *T cells and B cells colocalize in PDAC*

369 Although T cell infiltration is often assessed for its prognostic capacity, effective immunity requires
370 cooperation between immune cell subtypes. To determine whether additional cells might interact
371 with T cells in the tumour environment, we performed Spearman's correlation analysis on average
372 immune cell densities across patients. Positive correlations were observed between CD3+CD8– and
373 CD3+CD8+ T cells ($R = 0.64$, $p<0.001$), CD3+CD8– T cells and B cells ($R = 0.71$, $p<0.001$), and
374 CD3+CD8+ T cells and B cells ($R = 0.52$, $p<0.001$) **(Figure 5A)**. These findings suggest that crosstalk
375 may occur between lymphocytes, which may prompt formation of niches within the PDAC
376 microenvironment.

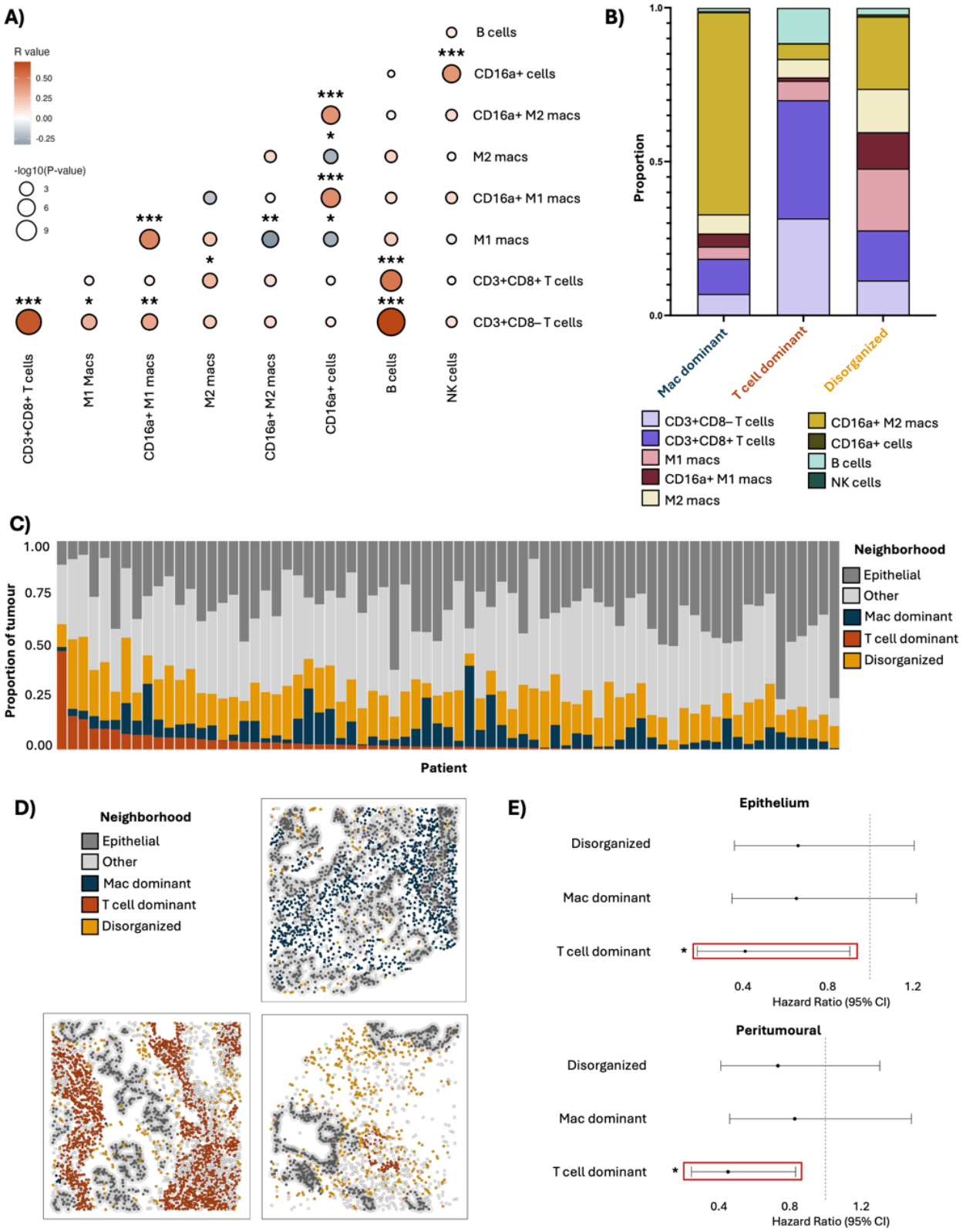

Figure 5. Co-infiltration and spatial organization of T cells and B cells is associated with improved patient outcomes in PDAC. (A) Co-infiltration of total cell densities in PDAC tumours,

380 determined by Spearman's correlation. Colour intensity indicates the strength of correlation, and dot
381 size reflects the statistical significance (p-value). **(B)** Cell type proportions comprising the three
382 immune neighbourhoods identified via spatial clustering. **(C)** Proportional representation of each
383 immune neighbourhood in each of the 73 tumours assessed **(D)** Representative spatial
384 neighbourhood maps demonstrating each neighbourhood subtype: Macrophage (Mac) dominant, T
385 cell dominant, and Disorganized. **(E)** Forest plots of hazard ratios and 95% confidence intervals from
386 univariate Cox regressions comparing "high" vs "low" proportions of each neighbourhood in the
387 intratumoural region. Solid red box indicates neighbourhood significant in both univariate and
388 multivariate models.
389

390 We next applied radius-based nearest neighbor clustering to ascertain potential interactions
391 between immune cell types. With these, we identified three patterns of immune cell colocalization,
392 which we termed "neighbourhoods". The first was a *macrophage dominant* neighbourhood,
393 composed primarily of CD16a+ M2-like macrophages, consistent with an immunosuppressive
394 function **(Figure 5B).** The second was a *T cell dominant* neighbourhood, enriched for CD3+CD8– T
395 cells, CD3+CD8+ T cells, and B cells, which may represent areas of organized adaptive immunity.
396 The third was a *disorganized* neighbourhood, characterized by a heterogenous mix of infiltrating
397 immune cells without a dominant cell type, suggestive of an unstructured (and perhaps inefficient)
398 immune response.

399 The relative area represented by each neighbourhood varied between patients; however, in
400 most tumours, the disorganized neighbourhood comprised the largest proportion of immune cells,
401 followed by the macrophage dominant neighbourhood, and then the T cell dominant neighbourhood
402 **(Figure 5C,D)**. The disorganized and macrophage dominant neighbourhoods were observed in all
403 patients, while the T cell dominant neighbourhood was present in ~90% of cases. Representative
404 examples of each neighbourhood pattern are shown in **Figure 5D**.

405 To evaluate whether immune neighbourhoods were associated with patient outcomes, we
406 performed Cox regression analyses comparing five-year OS in patients categorized as high or low for
407 each neighbourhood. Having a higher density of the T cell dominant neighbourhood in the epithelium
408 was associated with a decreased risk of death (HR: 0.41, 95% CI: 0.19-0.91, $p<0.05$). A higher

409 proportion of the T cell dominant neighbourhood within the peritumoural region was associated with
410 a decreased risk of death (HR: 0.45, 95% CI: 0.24-0.82, $p<0.05$) **(Figure 5E)**. These associations were
411 retained after multivariate Cox regression analysis **(Supplementary Table 3)**. Neither the
412 disorganized nor the macrophage dominant neighbourhoods were associated with OS. We conclude
413 that the spatial co-localization of T cells and B cells proximal to the tumour is prognostically
414 beneficial.
415

416 **Discussion**

417 PDAC tumours have a characteristically dense and desmoplastic stroma. The relative lack of anti-
418 tumour immune cells and highly immunosuppressive features are well-recognized.[4,5,40] These
419 observations have contributed to the prevailing view that PDAC may not be a suitable candidate for
420 immunotherapy. However, recent studies reveal pockets of immune cell localization in PDAC,[7]
421 suggesting that, at least in some regions, PDAC tumours may remain immunologically susceptible.
422 We profiled the immune landscape of 73 patients with PDAC, designing custom algorithms to assess
423 the tumours' unique ductal architecture. We found CD3+CD8- T cells to be associated with improved
424 five-year OS, particularly when they localize to the tumour-stroma interface and when they coincide
425 with CD3+CD8+ T cells in the tumour epithelium. T and B cell co-infiltration and co-localization were
426 associated with the longest OS, supporting our conclusion that productive antitumour immunity
427 results from the recruitment of cooperative immune cell types. This organization is consistent with
428 that of the "T cell dominant" neighbourhood, where it would be expected that cytotoxic T cell
429 immunity and antibody production could occur. This implies a susceptibility of PDAC to immune-
430 mediated mechanisms and sets type I immunity as a goalpost for its future immunotherapy.

431 Immune profiling using IHC, single-cell mass cytometry, and flow cytometry has
432 demonstrated that the extent and composition of T cell infiltration varies across patients with
433 PDAC.[37,38,41–43] Transcriptomic analyses identified distinct immunologic subtypes in PDAC, including
434 those that are immune-rich, immunosuppressive, immune-exhausted, or immune-depleted,
435 reflecting both the extent and functional state of immune infiltration.[6–10,38] While transcriptomic
436 subtypes reflect functional immune states, they do not fully capture the spatial heterogeneity
437 observed within individual tumours. Recent studies demonstrate that tumours are not universally
438 comprised of a single cell type or subregion.[7,44] This regional variation, "sub-TMEs", might reflect
439 PDAC's continued growth and diversification,[45,46] and possibly a co-evolution with immunity and

440 immune escape. We similarly observe a range of immune cell densities between patients, with
441 CD3+CD8– T cells (likely CD4+ T cells), CD3+CD8+ T cells, and CD16a+ M2-like macrophages
442 representing the dominant phenotypes in both the epithelial and stromal compartments. This is
443 consistent with previous studies demonstrating that T cells are often the most abundant immune
444 population in the PDAC stroma, even exceeding myeloid cells.[38,41,47] With spatial assessments, we
445 note that B cells are also included in these neighbourhoods, so the T cell populations are likely
446 harbingers of more complex local immunity.

447 Higher densities of CD3+CD8– T cells in the stroma and T cell dominant neighbourhoods
448 were associated with lengthened five-year OS. Due to limitations in panel size, we could not stain for
449 CD4 directly, but infer these to be the CD3+CD4+ helper T cell subset. Likewise, an assessment of
450 the features of CD4+ subsets is beyond the scope of our panel, but the co-localization of CD3+CD8-
451 cells with B cells, M1 macrophages and CD3+CD8+ cells suggests their contribution to a type I
452 immune response (likely associated with the Th1 helper cell subset). Since these cells associate with
453 a survival benefit, we expect that they represent CD3+CD8–CD4+Foxp3– effector cells, which are
454 known to correlate with improved survival in PDAC.[37] CD4+ T helper cells promote anti-tumour
455 immunity by orchestrating dendritic cell activation and licensing, facilitating CD8+ T cell recruitment,
456 and supporting B cell maturation.[25] Helper T cell localization near the tumour border may facilitate
457 direct tumour cell killing through the release of cytotoxic cytokines (e.g. interferon-γ and tumour
458 necrosis factor-α) or engagement of death receptors including TRAIL and FasL.[25,48,49] Since these
459 functions can occur even at a distance, our findings of benefit to OS of CD3+CD8– T cells in both the
460 stroma and at the peritumoural regions still support a conclusion that these cells function as helpers.

461 The prognostic significance of stromal CD3+CD8– T cells was further enhanced when
462 CD3+CD8+ T cells were also present within the epithelium. Indeed, CD3+CD8+ T cells rarely infiltrate
463 in the absence of CD3+CD8– T cells, underscoring that these helper populations may facilitate the

464 recruitment or maintenance of the CD8+ populations in PDAC. CD3+CD8– T cells, CD3+CD8+ T cells,
465 and B cells co-infiltrated and co-localized, comprising the primary cell types in the T cell-dominated
466 neighbourhood. This spatial arrangement could reflect tertiary lymphoid structure (TLS)-like
467 formations: organized groupings of immune cells that are associated with improved overall survival
468 in PDAC[50–52]. TLSs support antigen presentation and adaptive immune activation; within them,
469 interactions between B cells, CD4+ T cells, and CD8+ T cells – such as antigen presentation, co-
470 stimulation, and cytokine-mediated signalling – promote coordinated immune responses.[18]
471 Although we did not have the necessary markers to definitively classify our T cell dominant
472 neighbourhoods as TLSs, the composition of these two types of neighbourhoods is aligned, and their
473 positioning at the tumour and peritumoural regions in patients with longer OS supports a productive
474 anti-cancer immunity.

475 In addition to the T cell dominant neighbourhood, we defined two others: macrophage-
476 dominant and disorganized. These may reflect immune subtypes previously described in PDAC. For
477 example, the macrophage dominant neighbourhood, enriched for CD16a+ M2-like macrophages and
478 exhibiting minimal T and B cell presence, may reflect an immunosuppressive environment consistent
479 with previously defined "basal-like", "squamous", or perhaps even "immune escape".[6,53,54] The T cell
480 dominant neighbourhood could reflect the previously defined "immune rich", "reactive", or
481 "adaptive/T cell dominant" regions.[6–8] Finally, the disorganized environment might reflect the
482 "deserted" or "immune-exclusion/tumour dominant" tumour regions.[6,8]

483 PDAC has a distinctive histology in which tumour cells originate in the ducts and often spread
484 as small, irregular clusters that are often interspersed within dense stroma.[19,20] Existing approaches
485 for spatial assessments were insufficient to capture this architecture, and methodological choices
486 can influence interpretation. In our study, we first identified tumour clusters, then defined 30-μm
487 borders around these clusters to capture both immune-immune and immune-tumour interactions

488 occurring in their vicinity. This approach was designed to capture the histology of PDAC and improve
489 biological relevance by reflecting the context in which immune activity at the tumour-stroma
490 interface may be as relevant as direct tumour contact.[55,56] Other studies using different spatial
491 definitions (e.g. measuring immune cell proximity within 20-μm of each tumour cells) have reported
492 associations between CD8+ T cells in direct contact with tumour cells and patient outcomes.[37] This
493 approach provides insight into direct tumour-immune interactions, but may not capture the broader
494 immune context, including activity at the tumour-stroma interface. This may explain why CD4+ T cell
495 proximity was not similarly associated with survival in those studies, despite their overall findings
496 supporting the prognostic relevance of T cell infiltration.[37] Our analysis, which used a different
497 spatial framework, may reflect complementary aspects of PDAC histology and immune dynamics.
498 Most patients with PDAC are diagnosed at advanced stages, whereas our cohort consisted
499 only of patients who underwent surgical resection (stage I-IIIa). Our findings thus reflect earlier-stage
500 disease and may not fully capture the TME of metastatic PDAC. It is possible that patients with
501 metastatic disease harbour a distinct TME.[45] While we did not observe an association between
502 tumour stage and immune contexture, it remains possible that tumours evolve toward becoming
503 disorganized or immunologically-cold as they progress to advanced stages. Although functional data
504 were beyond the scope of this work, our findings support future investigations and possible
505 interventions to maximize the activity of the TLS-like/T cell dominant neighbourhoods in PDAC.
506

Acknowledgements

We thank the patients who generously donated tissue and clinical information for this study, as well as the Nova Scotia Health Biobank for their contributions to sample and data collection. We are grateful to Craig's Cause Pancreatic Cancer Society for their support. Dalhousie University and the Boudreau laboratory are situated in Mi'kmi'ki, the traditional and unceded territory of the Mi'kmaq. This work was supported by the Canadian Cancer Society's Innovation (#705275) and JD Irving Atlantic Canada (#707195) grants to JEB. Clinical database creation was supported by a Nova Scotia Health Operating Grant and a Queen Elizabeth II Health Science Centre Foundation private donation research grant. RJA and JPM are trainees in the Cancer Research Training Program of the Beatrice Hunter Cancer Research Institute. Funds for RA and JPM are provided by GIVETOLIVE, by the Kilpatrick Trust through the Dalhousie Faculty of Medicine 2023 Graduate Studentship program, and by the Terry Fox MOHCCN Health Informatics and Data Scientist Awards. Funds for RA's work is supported by the Rick Salsman Pancreatic Cancer Studentship Fund through the Dalhousie Faculty of Medicine 2025 Graduate Studentship program.

References

1. Halbrook CJ, Lyssiotis CA, Pasca Di Magliano M, Maitra A. Pancreatic cancer: Advances and challenges. *Cell*. 2023;186(8):1729-1754. doi:10.1016/j.cell.2023.02.014

2. Lu J, Jiang G. The journey of CAR-T therapy in hematological malignancies. *Mol Cancer*. 2022;21(1):194. doi:10.1186/s12943-022-01663-0

3. Carlino MS, Larkin J, Long GV. Immune checkpoint inhibitors in melanoma. *The Lancet*. 2021;398(10304):1002-1014. doi:10.1016/S0140-6736(21)01206-X

4. Ju Y, Xu D, Liao M miao, et al. Barriers and opportunities in pancreatic cancer immunotherapy. *npj Precis Onc*. 2024;8(1):199. doi:10.1038/s41698-024-00681-z

5. Hartupee C, Nagalo BM, Chabu CY, et al. Pancreatic cancer tumor microenvironment is a major therapeutic barrier and target. *Front Immunol*. 2024;15. doi:10.3389/fimmu.2024.1287459

6. Grünwald BT, Devisme A, Andrieux G, et al. Spatially confined sub-tumor microenvironments in pancreatic cancer. *Cell*. 2021;184(22):5577-5592.e18. doi:10.1016/j.cell.2021.09.022

7. Wartenberg M, Cibin S, Zlobec I, et al. Integrated Genomic and Immunophenotypic Classification of Pancreatic Cancer Reveals Three Distinct Subtypes with Prognostic/Predictive Significance. *Clinical Cancer Research*. 2018;24(18):4444-4454. doi:10.1158/1078-0432.CCR-17-3401

8. de Santiago I, Yau C, Heij L, et al. Immunophenotypes of pancreatic ductal adenocarcinoma: Meta-analysis of transcriptional subtypes. *Int J Cancer*. 2019;145(4):1125-1137. doi:10.1002/ijc.32186

9. Li R, He Y, Zhang H, et al. Identification and Validation of Immune Molecular Subtypes in Pancreatic Ductal Adenocarcinoma: Implications for Prognosis and Immunotherapy. *Front Immunol*. 2021;12. doi:10.3389/fimmu.2021.690056

10. Chen Y, Chen D, Wang Q, et al. Immunological Classification of Pancreatic Carcinomas to Identify Immune Index and Provide a Strategy for Patient Stratification. *Front Immunol*. 2022;12. doi:10.3389/fimmu.2021.719105

11. Personalized RNA neoantigen vaccines stimulate T cells in pancreatic cancer | Nature. Accessed October 14, 2025. https://www.nature.com/articles/s41586-023-06063-y

12. Sethna Z, Guasp P, Reiche C, et al. RNA neoantigen vaccines prime long-lived CD8+ T cells in pancreatic cancer. *Nature*. 2025;639(8056):1042-1051. doi:10.1038/s41586-024-08508-4

13. Li X, Gruosso T, Zuo D, et al. Infiltration of CD8+ T cells into tumor cell clusters in triple-negative breast cancer. *Proceedings of the National Academy of Sciences*. 2019;116(9):3678-3687. doi:10.1073/pnas.1817652116

14. Bull JA, Macklin PS, Quaiser T, et al. Combining multiple spatial statistics enhances the description of immune cell localisation within tumours. *Sci Rep*. 2020;10(1):18624. doi:10.1038/s41598-020-75180-9

15. Schürch CM, Bhate SS, Barlow GL, et al. Coordinated Cellular Neighborhoods Orchestrate Antitumoral Immunity at the Colorectal Cancer Invasive Front. *Cell*. 2020;182(5):1341-1359.e19. doi:10.1016/j.cell.2020.07.005

16. Nersesian S, Arseneau RJ, Mejia JP, et al. Improved overall survival in patients with high-grade serous ovarian cancer is associated with CD16a+ immunologic neighborhoods containing NK cells, T cells and macrophages. *Front Immunol*. 2024;14. doi:10.3389/fimmu.2023.1307873

17. Xu H, Cha YJ, Clemenceau JR, et al. Spatial analysis of tumor-infiltrating lymphocytes in histological sections using deep learning techniques predicts survival in colorectal carcinoma. *The Journal of Pathology: Clinical Research*. 2022;8(4):327-339. doi:10.1002/cjp2.273

18. Liu C, Cao J. The pivotal role of tertiary lymphoid structures in the tumor immune microenvironment. *Front Oncol*. 2025;15. doi:10.3389/fonc.2025.1616904

19. Kearney JF, Adsay V, Yeh JJ. Pathology and Molecular Characteristics of Pancreatic Cancer. *Surg Oncol Clin N Am*. 2021;30(4):609-619. doi:10.1016/j.soc.2021.06.003

20. Klöppel G, Adsay NV. Chronic Pancreatitis and the Differential Diagnosis Versus Pancreatic Cancer. *Arch Pathol Lab Med*. 2009;133(3):382-387. doi:10.5858/133.3.382

21. A Grammar of Data Manipulation. Accessed October 10, 2025. https://dplyr.tidyverse.org/

22. Type, Density, and Location of Immune Cells Within Human Colorectal Tumors Predict Clinical Outcome | Science. Accessed October 10, 2025. https://www-science-org.ezproxy.library.dal.ca/doi/10.1126/science.1129139

23. Galon J, Fridman WH, Pagès F. The Adaptive Immunologic Microenvironment in Colorectal Cancer: A Novel Perspective. *Cancer Res*. 2007;67(5):1883-1886. doi:10.1158/0008-5472.CAN-06-4806

24. Raskov H, Orhan A, Christensen JP, Gögenur I. Cytotoxic CD8+ T cells in cancer and cancer immunotherapy. *Br J Cancer*. 2021;124(2):359-367. doi:10.1038/s41416-020-01048-4

25. Borst J, Ahrends T, Bąbała N, Melief CJM, Kastenmüller W. CD4+ T cell help in cancer immunology and immunotherapy. *Nat Rev Immunol*. 2018;18(10):635-647. doi:10.1038/s41577-018-0044-0

26. Wolf S, Anastasopoulou V, Drousch K, et al. 403 A four-cell type interaction between CD4+ T cells, CD8+ T cells, stromal and cancer cells as a potential mechanism for cancer eradication when one CD4TCR is combined with one CD8TCR. *J Immunother Cancer*. 2024;12(Suppl 2). doi:10.1136/jitc-2024-SITC2024.0403

27. Ouyang P, Zhang J, He X, Yang C, Zeng D, Xu D. Infiltration characteristics and regulatory mechanisms of CD8+ T lymphocytes in solid tumors: spatial distribution, biological functions, and interactions with the immune microenvironment. *Front Immunol*. 2025;16. doi:10.3389/fimmu.2025.1661545

28. McKinney W. Data Structures for Statistical Computing in Python. In: 2010:56-61. doi:10.25080/Majora-92bf1922-00a

29. Harris CR, Millman KJ, van der Walt SJ, et al. Array programming with NumPy. *Nature*. 2020;585(7825):357-362. doi:10.1038/s41586-020-2649-2

30. Pedregosa F, Varoquaux G, Gramfort A, et al. Scikit-learn: Machine Learning in Python. *J Mach Learn Res*. 2011;12(null):2825-2830.

31. davies_bouldin_score. scikit-learn. Accessed October 10, 2025. https://scikit-learn/stable/modules/generated/sklearn.metrics.davies_bouldin_score.html

32. Hunter JD. Matplotlib: A 2D Graphics Environment. *Computing in Science & Engineering*. 2007;9(3):90-95. doi:10.1109/MCSE.2007.55

33. Journal of Open Source Software: seaborn: statistical data visualization. Accessed July 31, 2025. https://joss.theoj.org/papers/10.21105/joss.03021

34. Ester M, Kriegel HP, Xu X. A Density-Based Algorithm for Discovering Clusters in Large Spatial Databases with Noise.

35. Virtanen P, Gommers R, Oliphant TE, et al. SciPy 1.0: fundamental algorithms for scientific computing in Python. *Nat Methods*. 2020;17(3):261-272. doi:10.1038/s41592-019-0686-2

36. Sivakumar S, Jainarayanan A, Arbe-Barnes E, et al. Distinct immune cell infiltration patterns in pancreatic ductal adenocarcinoma (PDAC) exhibit divergent immune cell selection and immunosuppressive mechanisms. *Nat Commun*. 2025;16(1):1397. doi:10.1038/s41467-024-55424-2

622 37. Carstens JL, Correa de Sampaio P, Yang D, et al. Spatial computation of intratumoral
623 T cells correlates with survival of patients with pancreatic cancer. *Nat Commun*.
624 2017;8(1):15095. doi:10.1038/ncomms15095

625 38. Wang H, Chen L, Qi L, et al. A Single-Cell Atlas of Tumor-Infiltrating Immune Cells in
626 Pancreatic Ductal Adenocarcinoma. *Molecular & Cellular Proteomics*.
627 2022;21(8):100258. doi:10.1016/j.mcpro.2022.100258

628 39. Yu M, Guan R, Hong W, et al. Prognostic value of tumor-associated macrophages in
629 pancreatic cancer: a meta-analysis. *Cancer Manag Res*. 2019;11:4041-4058.
630 doi:10.2147/CMAR.S196951

631 40. Guo S, Wang Z. Unveiling the immunosuppressive landscape of pancreatic ductal
632 adenocarcinoma: implications for innovative immunotherapy strategies. *Front Oncol*.
633 2024;14:1349308. doi:10.3389/fonc.2024.1349308

634 41. Blando J, Sharma A, Higa MG, et al. Comparison of immune infiltrates in melanoma
635 and pancreatic cancer highlights VISTA as a potential target in pancreatic cancer.
636 *Proceedings of the National Academy of Sciences*. 2019;116(5):1692-1697.
637 doi:10.1073/pnas.1811067116

638 42. Stromnes IM, Hulbert A, Pierce RH, Greenberg PD, Hingorani SR. T-cell Localization,
639 Activation, and Clonal Expansion in Human Pancreatic Ductal Adenocarcinoma. *Cancer*
640 *Immunology Research*. 2017;5(11):978-991. doi:10.1158/2326-6066.CIR-16-0322

641 43. Steele NG, Carpenter ES, Kemp SB, et al. Multimodal mapping of the tumor and
642 peripheral blood immune landscape in human pancreatic cancer. *Nat Cancer*.
643 2020;1(11):1097-1112. doi:10.1038/s43018-020-00121-4

644 44. Hilmi M, Delecourt F, Raffenne J, et al. Redefining phenotypic intratumor
645 heterogeneity of pancreatic ductal adenocarcinoma: a bottom-up approach. *J Pathol*.
646 2025;265(4):448-461. doi:10.1002/path.6398

647 45. Li Y, Ding Z, Cheng T, et al. Single-cell transcriptomics analysis reveals dynamic
648 changes and prognostic signature in tumor microenvironment of PDAC. *Scientific*
649 *Reports*. 2025;15(1):4025. doi:10.1038/s41598-025-86950-8

650 46. Mullen KM, Hong J, Attiyeh MA, et al. The Evolutionary Forest of Pancreatic Cancer.
651 *Cancer Discov*. 2025;15(2):329-345. doi:10.1158/2159-8290.CD-23-1541

652 47. Shibuya KC, Goel VK, Xiong W, et al. Pancreatic Ductal Adenocarcinoma Contains
653 an Effector and Regulatory Immune Cell Infiltrate that Is Altered by Multimodal
654 Neoadjuvant Treatment. *PLOS ONE*. 2014;9(5):e96565.
655 doi:10.1371/journal.pone.0096565

48. Tateyama M, Oyaizu N, McCloskey TW, Than S, Pahwa S. CD4 T lymphocytes are primed to express Fas ligand by CD4 cross-linking and to contribute to CD8 T-cell apoptosis via Fas/FasL death signaling pathway: Presented in part at the 12th World AIDS Conference, Geneva, Switzerland, 1998. *Blood*. 2000;96(1):195-202. doi:10.1182/blood.V96.1.195

49. Thomas WD, Zhang XD, Franco AV, Nguyen T, Hersey P. TNF-Related Apoptosis-Inducing Ligand-Induced Apoptosis of Melanoma Is Associated with Changes in Mitochondrial Membrane Potential and Perinuclear Clustering of Mitochondria1. *The Journal of Immunology*. 2000;165(10):5612-5620. doi:10.4049/jimmunol.165.10.5612

50. Zou X, Lin X, Cheng H, et al. Characterization of intratumoral tertiary lymphoid structures in pancreatic ductal adenocarcinoma: cellular properties and prognostic significance. *J Immunother Cancer*. 2023;11(6):e006698. doi:10.1136/jitc-2023-006698

51. Hiraoka N, Ino Y, Yamazaki-Itoh R, Kanai Y, Kosuge T, Shimada K. Intratumoral tertiary lymphoid organ is a favourable prognosticator in patients with pancreatic cancer. *Br J Cancer*. 2015;112(11):1782-1790. doi:10.1038/bjc.2015.145

52. Lehmann J, Thelen M, Kreer C, et al. Tertiary Lymphoid Structures in Pancreatic Cancer are Structurally Homologous, Share Gene Expression Patterns and B-cell Clones with Secondary Lymphoid Organs, but Show Increased T-cell Activation. *Cancer Immunology Research*. 2025;13(3):323-336. doi:10.1158/2326-6066.CIR-24-0299

53. Bailey P, Chang DK, Nones K, et al. Genomic analyses identify molecular subtypes of pancreatic cancer. *Nature*. 2016;531(7592):47-52. doi:10.1038/nature16965

54. Moffitt RA, Marayati R, Flate EL, et al. Virtual microdissection identifies distinct tumor- and stroma-specific subtypes of pancreatic ductal adenocarcinoma. *Nat Genet*. 2015;47(10):1168-1178. doi:10.1038/ng.3398

55. Feng Z, Bethmann D, Kappler M, et al. Multiparametric immune profiling in HPV– oral squamous cell cancer. *JCI Insight*. 2(14):e93652. doi:10.1172/jci.insight.93652

56. Oyler-Yaniv A, Oyler-Yaniv J, Whitlock BM, et al. A Tunable Diffusion-Consumption Mechanism of Cytokine Propagation Enables Plasticity in Cell-to-Cell Communication in the Immune System. *Immunity*. 2017;46(4):609-620. doi:10.1016/j.immuni.2017.03.011

Data availability

The data generated and code used in this study are available upon request from the corresponding author.